

Article

Sewage Sludge Plasma Gasification: Characterization and Experimental Rig Design [†]

Nuno Pacheco ^{1,*}, André Ribeiro ¹, Filinto Oliveira ², Filipe Pereira ³, L. Marques ⁴, José C. Teixeira ⁵,
Cândida Vilarinho ⁵ and Flavia V. Barbosa ⁵

¹ CVR—Centre for Waste Valorization, University of Minho, 4800-042 Guimarães, Portugal; aribeiro@cvresiduos.pt

² NEL—New Energy Level, Lda., 4760-758 Vila Nova de Famalicão, Portugal; filinto.oliveira@newenergylevel.pt

³ Ambitrevó—Soluções Agrícolas e Ambientais, Lda., 2100-011 Coruche, Portugal; filipe.pereira@ambitrevovo.pt

⁴ CF-UM-UP—Physics Center of Minho and Porto Universities, University of Minho, Campus de Gualtar, 4710-057 Braga, Portugal

⁵ MEtRICs I&D Centre, School of Engineering, University of Minho, 4800-042 Guimarães, Portugal; jt@dem.uminho.pt (J.C.T.); candida@dem.uminho.pt (C.V.); flaviab@dem.uminho.pt (F.V.B.)

* Correspondence: npacheco@cvresiduos.pt

[†] This paper is an extended version of the paper entitled “An Experimental Setup for Plasma Gasification of Sewage Sludge”, presented at the 8th Thermal and Fluids Engineering Conference (TFEC), College Park, MD, USA, 26–29 March 2023.

Abstract: The treatment of wastewater worldwide generates substantial quantities of sewage sludge (SS), prompting concerns about its environmental impact. Various approaches have been explored for SS reuse, with energy production emerging as a viable solution. This study focuses on harnessing energy from domestic wastewater treatment (WWT) sewage sludge through plasma gasification. Effective syngas production hinges on precise equipment design which, in turn, depends on the detailed feedstock used for characterization. Key components of plasma gasification include the plasma torch, reactor, heat exchanger, scrubber, and cyclone, enabling the generation of inert slag for landfill disposal and to ensure clean syngas. Designing these components entails considerations of sludge composition, calorific power, thermal conductivity, ash diameter, and fusibility properties, among other parameters. Accordingly, this work entails the development of an experimental setup for the plasma gasification of sewage sludge, taking into account a comprehensive sludge characterization. The experimental findings reveal that domestic WWT sewage sludge with 40% humidity exhibits a low thermal conductivity of approximately 0.392 W/mK and a calorific value of LHV = 20.78 MJ/kg. Also, the relatively low ash content (17%) renders this raw material advantageous for plasma gasification processes. The integration of a detailed sludge characterization into the equipment design lays the foundation for efficient syngas production. This study aims to contribute to advancing sustainable waste-to-energy technologies, namely plasma gasification, by leveraging sewage sludge as a valuable resource for syngas production.

Keywords: gasification; plasma; reactor; sewage sludges



Citation: Pacheco, N.; Ribeiro, A.; Oliveira, F.; Pereira, F.; Marques, L.; Teixeira, J.C.; Vilarinho, C.; Barbosa, F.V. Sewage Sludge Plasma Gasification: Characterization and Experimental Rig Design. *Reactions* **2024**, *5*, 285–304. <https://doi.org/10.3390/reactions5020014>

Academic Editor: Dmitry Yu. Murzin

Received: 2 November 2023

Revised: 25 March 2024

Accepted: 3 April 2024

Published: 16 April 2024



Copyright: © 2024 by the authors. Licensee MDPI, Basel, Switzerland. This article is an open access article distributed under the terms and conditions of the Creative Commons Attribution (CC BY) license (<https://creativecommons.org/licenses/by/4.0/>).

1. Introduction

Sewage sludge (SS), the final byproduct of wastewater treatment plants (WWTPs), which handle domestic or industrial effluents, requires proper management or safe disposal [1]. According to the latest Eurostat data, in 2020, the 27 European Member States produced over 3.1 million tons (dry basis (d.b.)) of sewage sludge from WWTPs [2]. Currently, the predominant methods of handling SS from WWTPs in Europe include landfilling, incineration, or agricultural reuse as a soil amendment [3].

Another route for handling sewage sludge is energy recovery. Among the various available methods, plasma gasification has emerged as one of the most effective and

environmentally friendly approaches for both sludge treatment and energy generation [4,5]. Plasma gasification, an advanced thermochemical process, utilizes high temperatures and gas plasma to convert organic matter into high-quality synthetic gas. This process offers several advantages, including the efficient destruction of organic pollutants, the reduction of waste volume and mass, and energy recovery [6–8]. Due to the high temperatures and rapid product quenching, thermal plasma gasification minimizes the formation of toxic compounds during waste treatment [9]. Utilizing this technology, sewage sludge can be decomposed into two primary products: combustible synthesis gas and inert glassy slag, providing significant environmental benefits in terms of atmospheric emissions and slag toxicity control [6].

However, as plasma gasification is a relatively new technology, there are still gaps in our understanding of its performance and characteristics. Additionally, sewage sludge gasification also presents challenges [9,10], mainly due to the heterogeneity of this raw material. Some of these challenges are presented by Gao et al. [11], such as the low heating value (LHV) of the material, the cold gas efficiency (CGE), the carbon conversion efficiency (CCE), the greenhouse gas emissions, the high levels of ash production, the high energy costs due to the need for moisture reduction prior to gasification, and the requirement to recover phosphorus (P), nitrogen (N), and potassium (K) from the ash [11]. Additionally, issues related to the geometry and dimensions of the plasma gasification reactor are mentioned [9,10].

Another significant challenge arises from the production of tar during the gasification process. Typically, mechanical methods such as scrubbers or washing towers are employed to remove tar from the gas stream. However, these methods merely transfer the problem to a wastewater stream contaminated with tar. Therefore, a more effective approach involves tar conversion rather than mere removal. Given that tar yields can range from low to 10 wt% or more, they contain a substantial amount of energy. Plasma methods, despite being the most expensive in terms of investment and operational costs, offer distinct advantages over other conversion methods like thermal or catalytic techniques. Plasma methods can be seen as a hybrid approach, combining high temperatures typically associated with thermal methods and the presence of reactive species (e.g., radicals, electrons, ions, and excited molecules), which significantly enhance the decomposition process. This results in a high conversion rate of tar into valuable products, ultimately leading to an overall improvement in feedstock conversion [4].

Although limited, several studies have been conducted on the gasification of various types of sludge using plasma technology. The majority of these studies were conducted at the laboratory scale, employing arc electric torches [10,12], highlighting the need to explore and contribute to the research on sewage sludge plasma gasification processes [9,10].

In this work, an experimental setup for the plasma gasification of sewage sludges is presented. This study aims to contribute to advancing sustainable waste-to-energy technologies, namely plasma gasification, by leveraging sewage sludge as a resource for syngas production. By integrating a detailed sludge characterization into equipment design, we lay the foundation for efficient syngas production. A comprehensive understanding of sludge properties and their impact on equipment design is crucial for optimizing the plasma gasification process. Ultimately, our research aims to reduce the knowledge gap regarding the performance and characteristics of plasma gasification, particularly in the context of sewage sludge treatment.

2. Materials and Methods

This section describes the experimental setup used in the gasification of sewage sludge, the methodologies implemented to characterize the raw material and its ashes, and their utility in the design of the gasification reactor and its peripherals.

2.1. Experimental Setup

The experimental setup is based on four main parts, which are arranged according to the scheme illustrated in Figure 1, and include the gasification reactor, a heat exchanger, a gas scrubber, and a particle separator, connected in series. The gasification reactions occur in the reactor chamber. The raw material, the SS sample, will be inserted at half the distance from the reactor bottom and placed at the bottom wall of the reactor. The samples will be heated by a plasma torch which is located on the left-hand side wall at an angle of 30°. The plasma torch employed in this experimental setup is a commercially available transferred arc plasma torch, which is housed in a water jacket for cooling purposes. The power supply for the plasma torch is a RED STAR, model CUT 65.3, with an input power of 7.8 kW. For calculation purposes, a heating efficiency of 50% was applied, as mentioned in the work of Ali et al. [4]. The original plasma torch is designed to operate with compressed air (4.4–5.0 bar) as the process gas, with a flow rate ranging from 142 to 235 L/min. Both the air flow and the power of the plasma torch can be adjusted. The produced gas will be released at the top of the reactor and forwarded to a heat exchanger. This equipment will allow for the gas temperature to be reduced to avoid the formation of dioxins and furans. Then, the cold gas will follow to a venturi scrubber, which will allow fine particulates to be captured. The produced gas will finally enter a cyclone particle separator to remove water droplets and the remaining particles that travel with the gas.

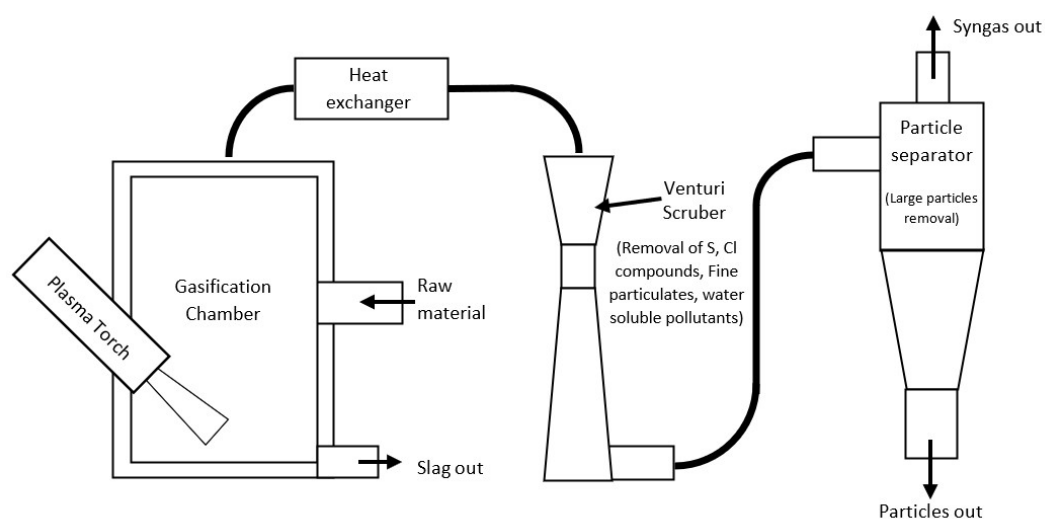


Figure 1. Experimental setup scheme.

To ensure an efficient gasification process and the production of high-quality syngas for energy generation, all equipment must be accurately designed. Therefore, the following sections present the design of each piece of equipment.

2.2. Sewage Sludge Characterization

2.2.1. Physicochemical Characterization

In this study, a sample of sewage sludge obtained from a strictly domestic wastewater treatment plant, located in the north of Portugal, was selected based on its gasification potential, as concluded by Pacheco et al. [12]. The sewage sludge sample was characterized in terms of the loss of humidity at 105 °C, volatile solids at 550 °C, and ashes at 800 °C, as well as the nitrogen (N), carbon (C), hydrogen (H), Sulphur (S), and low and high calorific value (LHV, HHV) it contained. Infrared absorption was used to determine the C, H, and S content, and the thermal conductivity method was used to determine N content. To determine the calorific values, an isoperibol bomb calorimeter was used.

2.2.2. Thermogravimetric Analysis

A Thermogravimetric Analysis (TGA) and Differential Scanning Calorimetry Analysis (DSC) were carried out to characterize the mass loss/gain in terms of function of temperature. This technique allows for the characterization of the thermal decomposition of the substances that comprise the sewage sludge. The experiments were performed using an SDT 2960 Simultaneous DSC-TGA equipment from TA Instruments (New Castle, DE, USA). To understand the influence of the atmosphere on the process, all samples were tested under an air atmosphere. The samples were heated to 1100 °C at a heating rate of 10 °C/min.

2.2.3. Thermal Properties

The thermal conductivity of the sewage sludge was measured using a hot disk TPS technique, depicted in Figure 2. The equipment uses a thin foil disk with a bifilar spiral pattern made of nickel involving Kapton mica sheets, which act as both the temperature sensor and the electrical resistive heater [13]. To conduct the experiments, the sensor is sandwiched between two identical pieces of the same sample that is to be tested. The sample geometry is defined based on the reference geometry presented in the system manual, as schematically presented in Figure 1. During the experiments, stepwise heating is produced by applying a stepwise current to the sensor, inducing a dynamic temperature field over the sensor and samples, which is monitored over time. By recording the variation in the sensor resistance, it is also possible to obtain the increase in temperature as a function of time, which is related to the thermal properties of the sample [14], according to Equation (1):

$$\Delta T(\tau) = P_0 \left(\pi^{\frac{3}{2}} r k \right)^{-1} D(\tau) \quad (1)$$

where $\Delta T(\tau)$ is the time-dependent temperature increase of the hot disk sensor; r is the radius of the sensor; k is the thermal conductivity of the sample; $D(\tau)$ is a dimensionless time function that accounts for the conduction pattern of the hot disk sensor, as defined by [15]. An important consideration regarding this technique is that the sensor is assumed to be placed in an infinite medium, so the propagation of the generated heat does not reach the boundaries of the sample throughout the experiment. This is an important factor to take into consideration during the definition of the sample dimensions. In this technique, the increase in the temperature of the sensor during the transient period should be linearly proportional to $D(\tau)$. Thus, ΔT can be fit as a function of $D(\tau)$, the characteristic time θ can be used as a fitting parameter, and the best value is used to calculate the thermal diffusivity according to Equation (2). The slope of the line corresponds to the factor $P_0 \left(\pi^{\frac{3}{2}} r k \right)^{-1}$, which is applied to obtain k .

$$\tau = \left(\frac{t}{\theta} \right)^{\frac{1}{2}}, \text{ where } \theta = \frac{r^2}{\alpha} \quad (2)$$

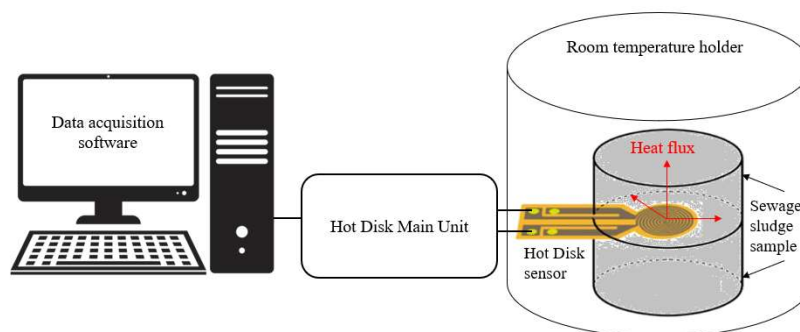


Figure 2. Experimental setup for thermal conductivity measurements of the sewage sludge.

2.3. Sewage Sludge Ashes Characterization

2.3.1. Chemical Composition

X-ray fluorescence spectroscopy (XRF) is widely used to analyze the chemical composition of sewage sludge ash. This non-destructive and sensitive technique allows for the identification and quantification of elements, including heavy metals and trace elements, providing crucial information for assessing environmental impacts, identifying toxic substances, and developing effective management and treatment strategies for these residues. In this work, the ash sample was analyzed using HITACHI equipment (Tokyo, Japan), model EA1000VX.

2.3.2. Particles Diameter

Measuring the ash's diameter is important to define the operating conditions and sizing of the scrubber and cyclone, since these equipment are used to remove the particles from the produced gas. To measure the particle's diameter, a Laser Diffraction Technique (LDT) is applied using a Malvern 2600. LDT, as depicted in Figure 3, uses a low-power He-Ne laser that forms a collimated beam of light. When the beam strikes a particle, light is scattered and collected by a receiver lens, which operates as a Fourier transform lens, forming the far-field diffraction pattern of the scattered light at its focal plane. The scattered light is gathered over a range of solid scattering angles by a detector that consists of 31 concentric annular sectors. The unscattered light goes into a small aperture and is monitored to define the volume and concentration of the sample. As the particle size decreases, the diffraction angle increases, and the quantification of the intensity of the diffracted beam at any angle allows for the number of particles to be determined [16]. The measured size range depends on the focal length of the lens, which can be extended from 0.5 μm up to 2 mm diameters with a dynamic range (d_{max}/d_{min}) of approximately 100. A size range varying between 100 and 10,000 particles is recommended to ensure accurate measurements.

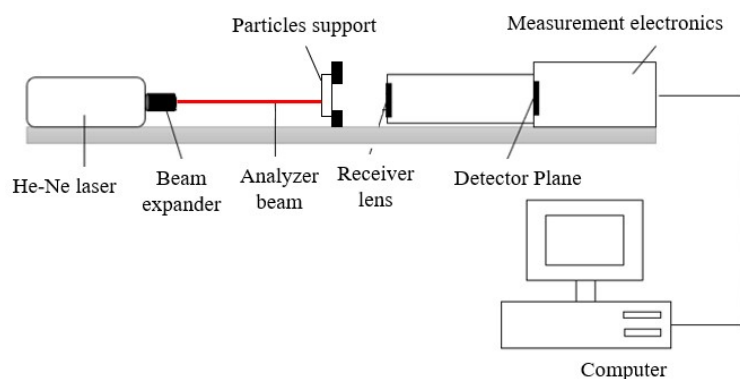


Figure 3. Experimental setup for sewage sludge ash diameter measurements.

The measurements are conducted in two steps to discard the influence of the external light sources. In this context, the background light was measured prior to the introduction of the particles, and its contribution was subtracted from the sample measurement. The ashes particles are mixed with water and pass through a solid particle support equipped with quartz windows that allow for optical access to the sample.

To conduct a data analysis, Malvern 2600 uses the Model Independent Analysis that estimates the volume distribution based on the measured light energy, assuming a 15-degree polynomial, from which the new light energy distribution is calculated using Equation (3) while the residual difference is obtained from Equation (4):

$$D_j = U_{i,j}V_i \quad (3)$$

$$\text{Log } D = \text{Log}_{10} \left(\sum (D_j - L_j)^2 \right) \quad (4)$$

where D_j is the measured data; V_i is the relative volume of material contained in the particles in size bands i and L_j ; the data were calculated from the estimated volume distribution. A new set of values of L_j is determined using the difference between D_j and L_j . This is an iterative process that ends as soon as the residual reaches a minimum value.

The measurement data correspond to the volume distribution of the material in the 32 bands, which is converted into a diameter. The derived diameter that is usually used in this context is the Sauter Mean Diameter (SMD), $D_{3,2}$, given by Equation (5) [17].

$$D_{3,2} = \frac{\sum n_i d_i^3}{\sum n_i d_i^2} \quad (5)$$

where d_i is the mean diameter of size band i ; m and n are subscripts that take the value 3 if a representation of the diameter in terms of volume is desired and a value of 2 for the surface.

2.3.3. Fusibility Evaluation

The fusibility of sewage sludge ash is an important property to consider in the management of these residues, as it affects both the efficiency of the treatment processes and the operation of associated equipment and systems [8], namely the fusibility of ash, which determines its ability to melt and flow. If the slag is excessively fusible, it can adhere to the internal surfaces of the gasifier, causing obstructions and reducing the process efficiency [18]. To characterize the ash melting behavior, several parameters were assessed, namely the shrinking starting temperature, deformation temperature, sphere temperature, hemisphere temperature, and flow temperature. These parameters were assessed in an external accredited laboratory. The applied methodology was in accordance with DIN 51730:2022-02 [19].

2.4. System Design

2.4.1. Reactor

The reactor is the most important part of the system since it is responsible for the efficiency of plasma gasification. The reactor's chamber is made from refractory cement and has a 340 mm diameter (D) and 1020 mm height, applying the height-to-diameter ratio of 3:1, according to [20], leading to an internal volume of 93 L.

Additionally, the specific flow rate of the treated sewage sludge was carefully considered during the design optimization process to ensure the optimal performance and efficiency of the plasma gasification system. This rate was determined based on a typical load for an updraft gasifier of 150 kg/m²/h, as reported by Prabir Basu [20], resulting in 15 kg/h in this specific case.

One of the most relevant properties related to plasma gasification is the position angle of the plasma torch. To ensure effective plasma gasification, it is important to optimize the plasma torch length, and the orientation angle plays an important role in this context. Therefore, the influence of the plasma torch position angle was analyzed numerically using the ANSYS FLUENT 2020 R2 software. The methodology that was implemented to conduct this study is presented below.

Simulation Domain and Meshing

The simulation domain adopted for flow modelling and reactor design optimization is depicted in Figure 4. These domains were meshed using ANSYS FLUENT, and refinement was conducted at the flow inlet, which corresponds to the nozzle of the torch with a diameter of 5 mm, as shown in Figure 5. For model simplification, the outlet diameter was converted into a hydraulic diameter of a square surface at the top of the gasifier. To ensure the quality of the meshes, different parameters were evaluated to ensure that mesh quality fell within the required values: skewness near zero; aspect ratio and element quality close to one.

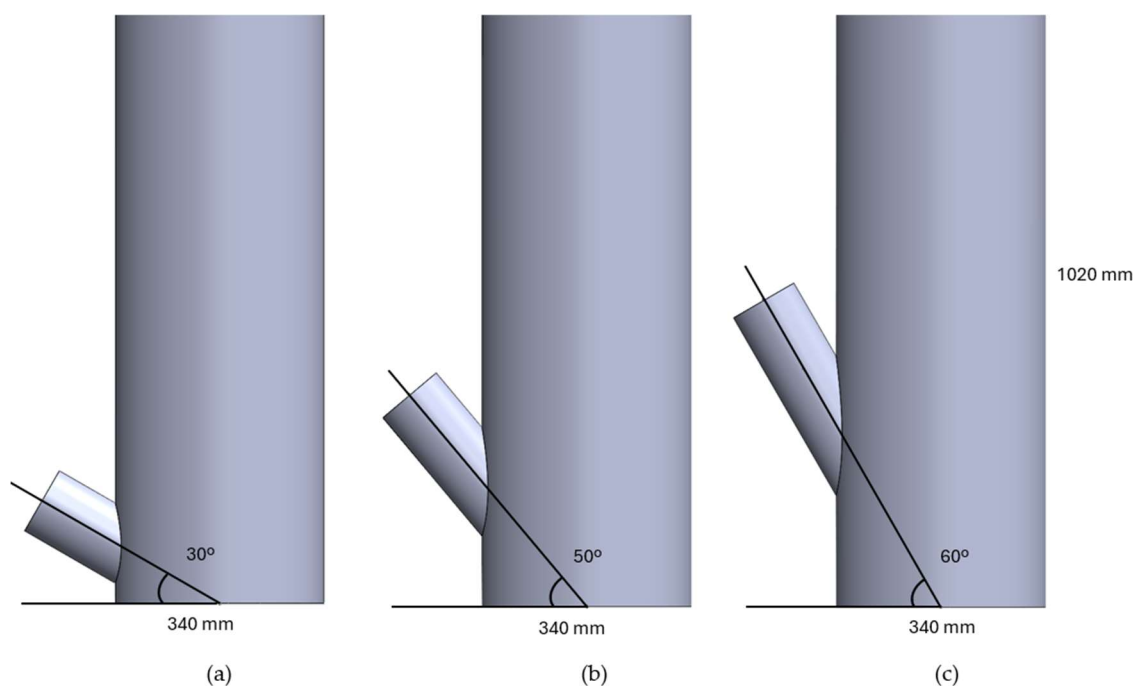


Figure 4. Reactor numerical domain for different position angles: (a) 30°; (b) 50°; (c) 60°.

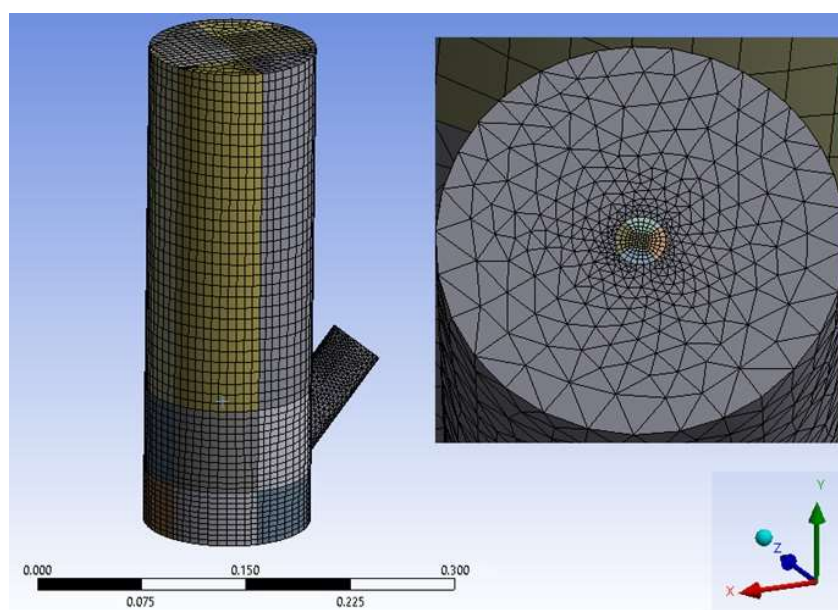


Figure 5. Meshed domain.

The boundary conditions implemented in this model are hot air injection at the circular nozzle of the torch at a temperature of 2726.85 °C and constant velocity, leading to a Reynolds number of approximately 1552. The induced jet flows inside the reactor and mix with the ambient air, before moving up through the outlet, defined as the pressure outlet boundary condition. The walls are defined by adiabatic and no-slip boundary conditions.

Governing Equations

ANSYS FLUENT 2020 R1 was applied to solve the Reynolds-averaged Navier–Stokes (RANS) equations set (6–9), where Equation (6) is the continuity, Equation (7) is the momentum, and Equation (8) is the energy equations. The low is assumed to be incompressible, since a Mach number below 0.3 was ensured in all simulations. Once the flow is in the

transition regime, the SST k - ω turbulence model, developed by Menter [21], is selected. This turbulence model is considered by several authors as an accurate model to simulate jet flows at low computational costs [22–27]. The equations used to solve turbulence kinetic energy, k , and the specific dissipation rate, ω , are presented in Equation (9) and Equation (10), respectively.

$$\nabla \cdot u = 0 \quad (6)$$

$$\frac{\partial u}{\partial t} + (u \cdot \nabla)u = -\frac{1}{\rho} \nabla p + \mu \nabla^2 u \quad (7)$$

$$\frac{\partial T}{\partial t} + u \cdot \nabla T = \alpha \nabla^2 T \quad (8)$$

$$\frac{\partial}{\partial t}(\rho k) + \frac{\partial}{\partial x_i}(\rho k u_i) = \frac{\partial}{\partial x_j} \left(\Gamma_k \frac{\partial k}{\partial x_j} \right) + G_k - Y_k + S_k \quad (9)$$

$$\frac{\partial}{\partial t}(\rho \omega) + \frac{\partial}{\partial x_i}(\rho \omega u_i) = \frac{\partial}{\partial x_j} \left(\Gamma_\omega \frac{\partial \omega}{\partial x_j} \right) + G_\omega - Y_\omega + S_\omega + D_\omega \quad (10)$$

where u is the velocity vector, p is the fluid pressure field, and T is the temperature. ρ , μ , and α are the constant physical properties of the fluid and represent the density, kinematic viscosity, and thermal diffusivity, respectively. Γ is the effective diffusivity, G is the generation, and Y is the dissipation of the corresponding variables; S is the user-defined source terms, while D_ω is the cross-diffusion term [28]. These variables were defined for air at a temperature of 2726.85 °C, according to [29].

The spatial discretization of diffusion and convective terms is solved using a second-order upwind scheme. To compute the face values of pressure from the cell values, a second-order interpolation scheme is implemented using a central differencing scheme. Pressure–velocity coupling is applied to derive an additional condition for pressure, and a procedure similar to that outlined by Rhie and Chow [30] is used to prevent checkerboarding [31]. The pressure-based solver uses a SIMPLE method to couple the pressure and velocity. The simulation is transient, so the governing equations are discretized in time through a first-order implicit integration. To perform the transient calculations, a fixed time step of 1×10^{-5} was applied.

Grid Sensitivity Analysis

To estimate the accuracy of the numerical results, a mesh sensitivity analysis was conducted using three different grid sizes. The number of cells selected for each case is presented in Table 1, varying between coarse, medium, and fine grids.

Table 1. Grid size.

Grid	N° Cells
Coarse	210,632
Medium	300,768
Fine	606,733

A grid sensitivity analysis was conducted for the velocity at the jet axis coming from the plasma torch normalized by the maximum recorded velocity value. The results depicted in Figure 6 show that the different velocity profile follows the same profile. However, the velocity values are slightly underestimated by the medium and coarse grids. The maximum deviations from the data predicted by the fine mesh are 15% and 35% for the medium and coarse mesh, respectively. Looking at the medium grid, it seems that 15% is not very significant, considering that the simulation time is reduced by half compared with the fine mesh. In this context, this grid was selected to conduct the numerical study.

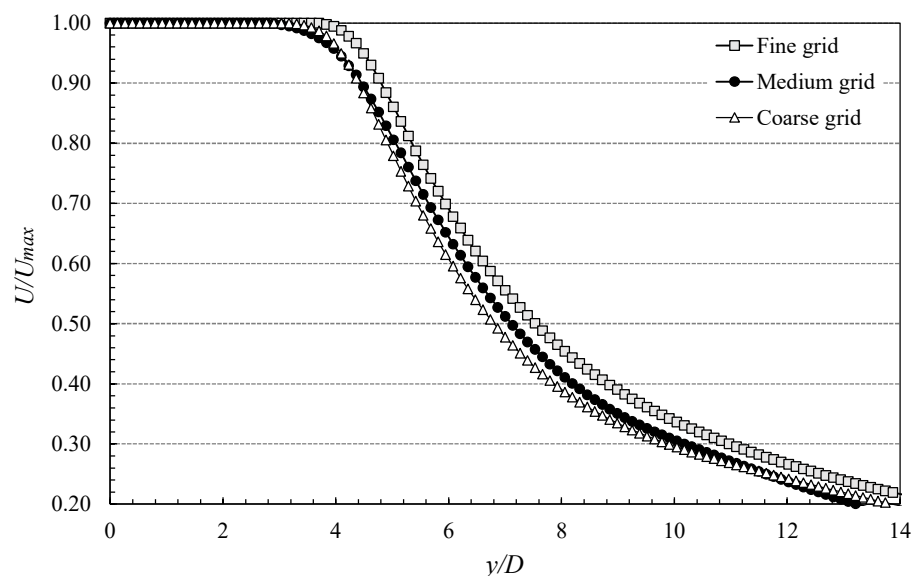


Figure 6. Grid sensitivity analysis.

2.4.2. Heat Exchanger

Considering the need for a very quick cooling of the gas coming from the reactor, a proper heat exchanger (HE) was developed to avoid the formation of dioxins and furans. The main factors commonly cited as facilitating the generation of these compounds are the low combustion temperatures (below 900 °C), a residence time in the furnace of below 1.5 s, and the high CO content (>100 ppm in the chimney, referred to 7% O₂), among others [32]. Also, according to [33], dioxins and furans are formed in regions after the combustion zone at lower temperatures, approximately between 180 and 550 °C.

Based on these assumptions, a shell-and-tube heat exchanger was designed. Taking into account the temperature and gas flow at the exit of the reactor (1000 °C, 0.16 m³/s), the residence time in the heat exchanger should be <1.5 s, and the desired temperature at the exit of the heat exchanger is 80 °C. As a cold fluid, a continuous flux of 15 L/min of water at 15 °C was considered.

The material available in the company for HE construction was a limitation. However, despite its unusual dimensions, the available tube was considered for the design of this component. Specifically, for the gas side, stainless steel tubes with an external diameter (d) of 25 mm and 2.5 mm thickness were considered. This has an influence on the compactness of the component, since this thickness seems to be excessive for the pressure level involved, in addition to the increase in thermal resistance.

For the design of the HE, the formulations of the one-shell pass and one-tube pass in a counter-flow heat exchanger, as proposed by Çengel [34], were used.

2.4.3. Scrubber

The scrubber is an important component to remove particle matter and acid gases from the gas streams. These pollutants are removed by impact, diffusion, and absorption using liquid droplets [35]. After the capture of these pollutants, the liquid is then collected for disposal. In this specific application, the collection will be performed by a cyclone located downstream of the scrubber. To ensure the high efficiency of the collection, a venturi jet scrubber was selected, since this allows for the capture of small particles (>1.0 µm) and allows for a wider range of liquid-to-gas ratios [36].

To design the venturi scrubber, a compromise between low-pressure losses and high collection efficiency must be ensured. To conduct this analysis, the 1D model developed by Azzopardi and Govan [37] to predict the total number of particles removed at each axial position of the throat was used. In this study, the throat diameter was fixed at 40 mm and the volumetric flow rate that was considered is equal to the one coming from the

reactor, i.e., $0.01625 \text{ m}^3/\text{s}$. The liquid-to-gas ratio is equal to $3 \text{ L}/\text{m}^3$, which lies under the range of recommended values for a venturi scrubber [36]. The velocity of the droplets was defined as equal to half of the gas velocity, as stated by Howard and Mohan [38], corresponding to $6.5 \text{ m}/\text{s}$, while the Sauter mean diameter of the atomized droplets was defined by the Nukisayama–Tamasawa equation presented by [38]. From this equation, the diameter of the obtained droplets was approximately $475 \text{ }\mu\text{m}$. To verify if the droplet velocity and diameter fell between the reference values used in commercially available atomizers, the study conducted by Miller et al. [39] was referred to, and the obtained values were validated.

2.4.4. Particle Separator

After being produced, the gas leaves the reactor and cools down in the HE. After that, it is forwarded to the wet scrubber whose function is to capture particles in the liquid droplets, removing them from the gas stream. However, to ensure the complete removal of particles that were not captured by the scrubber, as well as the droplets that may persist in the gas stream, a cyclone separator was introduced.

The sizing of this device was based on the formulations proposed by [40,41]. The proceeding started with the characterization of the particle ashes, namely their size and their density, as described later. As a result of that characterization, a minimum particle size of $5 \text{ }\mu\text{m}$ (with a density of $1.143 \text{ kg}/\text{m}^3$) was considered for the calculations. In addition to these parameters, a gas flow rate of $0.01625 \text{ m}^3/\text{s}$ at $80 \text{ }^\circ\text{C}$ was also taken into account when sizing a Lapple cyclonic separator.

3. Results and Discussion

3.1. Sewage Sludge Characterization

3.1.1. Physicochemical Characterization

The results of the ultimate and proximate analysis of the sewage sludge are presented in Figure 7. In the energy recovery of sewage sludges, the calorific value, humidity, and ash are parameters of particular importance. Regarding the LHV and HHV, the results obtained from the measurements on a dry basis (db) are $20.78 \text{ MJ}/\text{kg}$ and $22.59 \text{ MJ}/\text{kg}$, respectively.

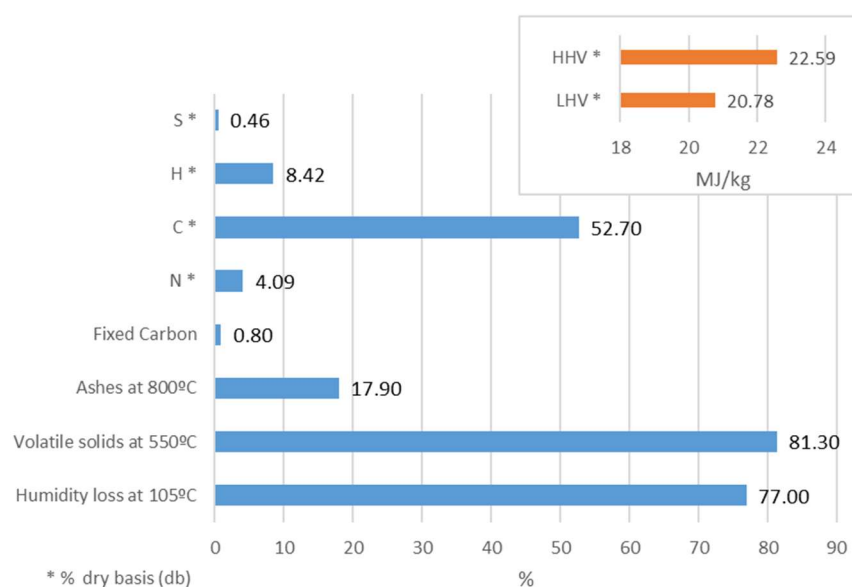


Figure 7. Ultimate and proximate analyses of sewage sludge sample.

Focusing on the data expressed in Figure 7, the percentage of loss of humidity at $105 \text{ }^\circ\text{C}$, volatile solids at $550 \text{ }^\circ\text{C}$, ashes at $800 \text{ }^\circ\text{C}$, and N, C, H, and S contents show that the sample has a high percentage of volatile solids, low ash content, and higher values of C and H. These are important properties for the heating value and the composition of the gas

produced in a gasifier [20]. Regarding the percentage of moisture, the sample presents a value greater than 70%. This sludge characteristic is relevant for plasma gasification since a high moisture content enhances the gasification process [11,42]. In terms of ash percentage, the results show that it is around 17.9%, which is an acceptable value when compared to the typical ash content found in the literature on sewage sludges [11,20,43,44]. The low fixed carbon content can be attributed to the predominance of organic materials and their rapid decomposition during wastewater treatment [45].

3.1.2. Thermogravimetric Analysis

The results of the DSC/TGA are presented in Figure 8. The variation in the mass loss as a function of temperature shows a reduction of about 80% of the total mass within the range of 200–600 °C when using air as an oxidizing atmosphere. This high value is mainly related to the higher reaction rate induced by the increased volatile matter content. Regarding the heat flow variation as a function of temperature, the results show two peaks that characterize the occurrence of different reactions. The first peak is expected to be due to the combustion of volatile matter, while the second one characterizes the combustion of char or fixed carbon. According to [46], the uncertainty in this experiment can be considered equal to 3.4%.

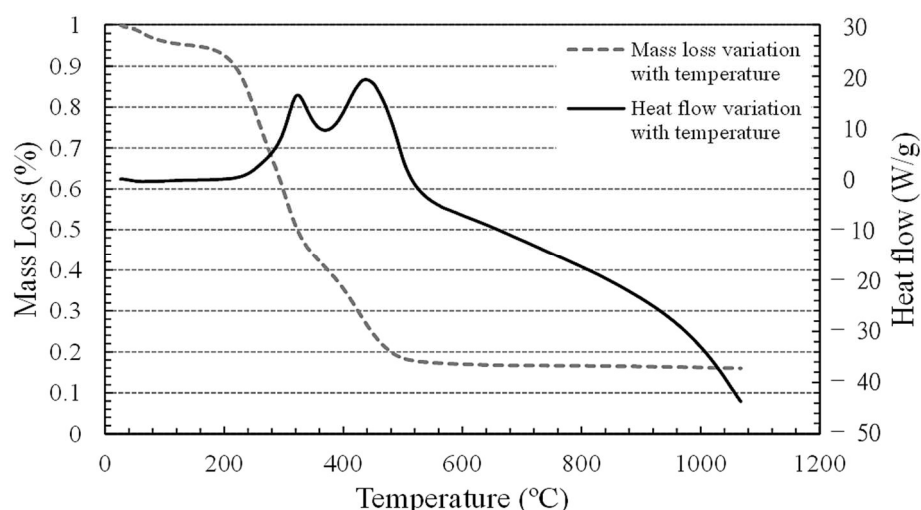


Figure 8. DSC/TGA measurements: mass loss and heat flow as a function of temperature.

3.1.3. Thermal Properties

The thermal properties obtained from the hot disk measurements correspond to the dry sewage sludge, and the results are expressed in the first line of Table 2. However, the sewage sludge that will be used for gasification has 40% humidity. With this percentage, it is not necessary to introduce steam inside the reactor to improve the production of hydrogen content. Therefore, the final thermal properties of the sample are a combination of 60% of the properties of the dry sample and 40% of the properties of water at 20 °C. The results are expressed in the final line of Table 2. Regarding thermal conductivity, the low value is also presented by [47,48].

Table 2. Thermal properties of the sewage sludge.

Material/Properties	k (W/mK)	α (mm ² /s)	C_p (J/kgK)	ρ (kg/m ³)
Dry sewage sludge	0.2498	0.1696	1172	1257
Water at 25 °C	0.607	1.457×10^{-3}	4180	997
Sewage sludge with 40% humidity	0.392	0.102	2375	1153

3.2. Sewage Sludge Ashes

3.2.1. Chemical Composition

The sewage sludge ashes' chemical characterization is presented in Table 3. The results show a high concentration of Silica (SiO_2), calcium (Ca), aluminium (Al), potassium (K), sodium phosphorus (P), sulfur (S), and trace elements like zinc (Zn) and copper (Cu). The high aluminium concentration can be explained by the flotation process in wastewater treatment. The remaining elements are related to the typical composition of the sewage sludge.

Table 3. Ashes' chemical composition.

Chemical Compound	% Mass	Chemical Compound	% Mass
CaO	15.8	P_2O_5	13.4
Fe_2O_3	5.5	Cl	0.07
SiO_2	38.1	S	1
Al_2O_3	17	SrO	0.05
MgO	2.3	Ni	0.04
MnO	0.09	RbO_2	0.04
TiO_2	1.7	Cu	0.45
Na_2O	<0.1	Zn	1.16
K_2O	3.4	Cr	0.05

3.2.2. Particle Diameter

The results recorded by the Malvern 2600 are expressed in terms of volume distribution. Considering previous knowledge about the mean diameter of smoke particles, the lens selected for the measurement was 63 mm, since the measuring range lies between 0.5 μm and 100 μm . Sauter Mean Diameter was applied to determine the particle size. This method does not contain the number of particles, but instead indicates around which central point of the frequency (surface area or volume/mass) the distribution varies [49]. From this analysis, it was estimated that $D_{3,2} = 36.23 \mu\text{m}$, while the minimum particle size that was recorded is equal to 11.6 μm . This last value is the reference needed to design the equipment integrated in the experimental setup.

3.2.3. Fusibility Characterization

The results of the fusibility characterization study provide valuable insights into the thermal behavior and melting properties of sewage sludge ash, crucial for its application in waste management and utilization processes. The results obtained are condensed in Table 4. According to the results of the thermal simulation presented earlier, the temperature achieved in the zone where the feedstock will be deposited remains around 1467 °C. As the ash's flow temperature is 1350 °C, the conditions inside the reactor will be suitable to ensure the complete fusion of the material.

Table 4. Ash melting behavior.

Parameter	Value (°C)
Shrinking starting temperature, tS	970
Deformation temperature	1210
Sphere temperature	1230
Hemisphere temperature	1270
Flow temperature	1350

The characterization of the sewage sludge and ashes provides relevant information for the appropriate design and construction of a plasma gasification setup. Based on these data, the reactor, scrubber, and cyclone were designed to ensure the production of an optimized syngas that can be used for energy production.

3.3. System Design

3.3.1. Reactor

The numerical results regarding the influence of the torch angle are presented in this section. Starting with the flow dynamics inside the reactor, the results depicted in Figure 9 show that, as the torch inclination increases, the distance of the air jet to the surface also increases; this occurs because the distance between the torch and the central axis of the reactor should be kept constant for all cases. In that sense, the results demonstrate that the lower left corner of the reactor has a great influence on flow development. As the angle increases, a recirculation region is induced in this location, interfering with the flow of the hot air jet that comes from the torch. This interference leads to instabilities along the wall where the waste will be deposited, and a greater temperature gradient and consequent decrease in heating efficiency are expected. Therefore, and since this recirculation is not identified when the torch is tilted at 30° , it is expected that more controlled and higher temperature and velocity values will be recorded.

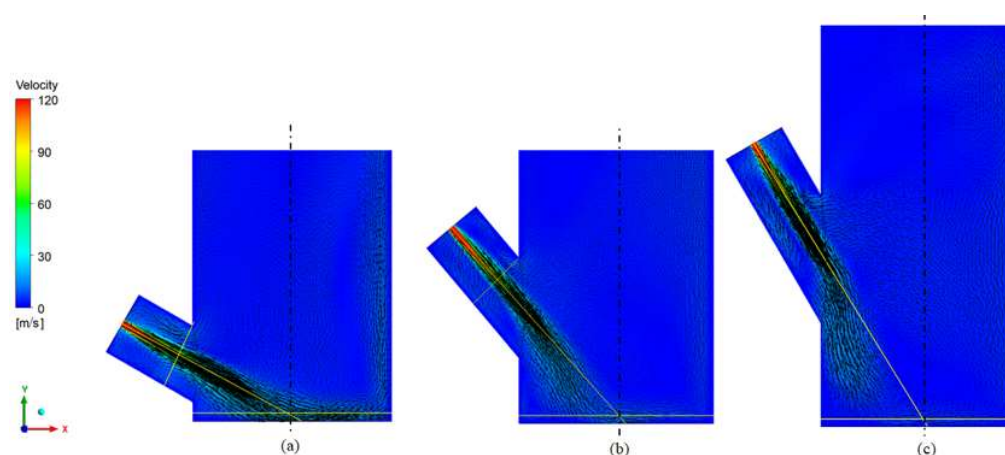


Figure 9. Flow profile inside the reactor: (a) 30° ; (b) 50° ; (c) 60° .

Looking at the development of the streamlines inside the reactor expressed in Figure 10, it can be seen that the development of the vortices inside the reactor varies depending on the torch angle. For higher angles, larger vortices are generated inside the reactor, allowing for an effective mixture between the hot air coming from the torch and the ambient air. The results, now referring to the xz plane presented in Figure 11, clearly show the asymmetrical geometry of these vortices, which does not occur with such intensity in the case of the 30° angle. However, these large structures interact with the flow of the plasma jet, leading to a reduction in velocity, as will be demonstrated by further results.

To quantitatively compare the results, the velocities normalized by the maximum velocity were evaluated for each case: 30° , 50° , and 60° . For this analysis, three graphs were constructed that represent the variation in velocity at different regions: along the jet axis, as shown in Figure 12a, next to the intersection zone between the reactor chamber and the torch outlet, as shown in Figure 12b, and next to the target surface at a distance corresponding to $y = 5$ mm, as shown in Figure 12c. The velocity profile allows for the characterization of the flow inside the reactor, and an analysis was conducted of the influence of the angle of inclination of the torch. A similar flow dynamic was observed for the three cases: a plume with a structure typical to a free jet flow, with maximum velocities recorded at the jet axis and a shear layer induced by the interaction of the jet flow and the surrounding air. The jet flows to the reactor's main chamber and decreases in velocity. Looking at Figure 12a, the jet potential core ends ($U/U_{max} < 0.95$) at a distance from the nozzle near $y/D = 2.7$ for 30° , $y/D = 4.2$ for 50° , and $y/D = 4.6$, for 60° , which is typical in jet flows [50,51]. The major reason for this difference is mainly related to the increased distance between the plasma torch inlet and the bottom of the reactor. However, the results show that the average

velocity for an inclination of 30° is approximately 22% and 40% higher than that at 50° and 60° , respectively. Once the jet enters the main chamber, it is deflected and only a portion of the mainstream flux reaches the center of the reactor (where the sample will be placed). A vortex is induced at the bottom left-hand side of the reactor, which grows higher with an increase in the inclination angle. This vortex leads to an asymmetry of the jet flow, with higher velocities recorded at the left-hand side of the jet axis. This asymmetry will cause a temperature non-uniformity that will interfere with the heating of the sample; thus, the higher the angle, the greater the thermal non-uniformity inside the reactor chamber. After impinging the reactor bottom wall, a non-uniform wall jet region is induced, as is clearly observed in Figure 12c. The velocity peak corresponds to approximately 18%, 8%, and 4% of the maximum velocity for 30° , 50° , and 60° , respectively. This peak is recorded near the stagnation region ($x/D = 0$), and a non-uniform velocity profile is recorded as the flow goes through the right-hand side of the reactor. From these results, it can be concluded that higher velocities are observed close to the target surface when the torch is tilted at 30° . These data corroborate previous observations that demonstrated that high angles of inclination of the torch induce vortices of greater magnitude and intensity, which interfere with the jet, leading to its degradation and a consecutive decrease in velocity.

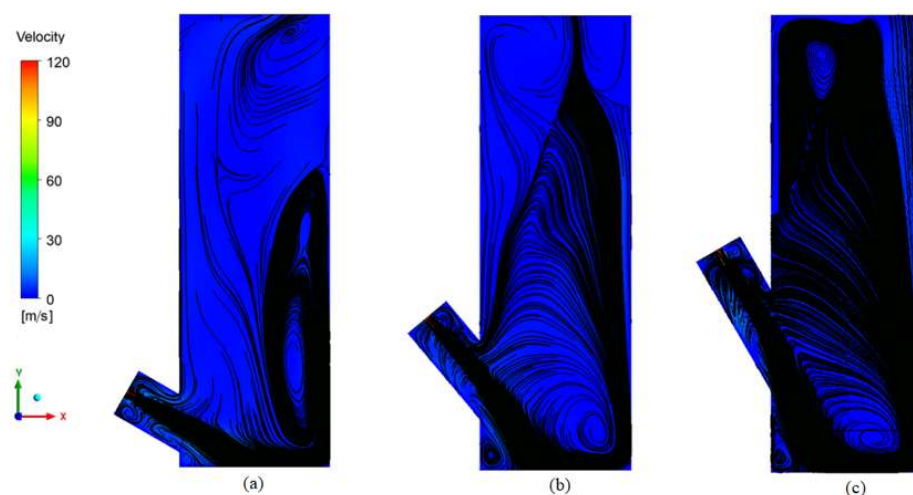


Figure 10. Streamlines inside the reactor chamber, according to the xy plane: (a) 30° ; (b) 50° ; (c) 60° .

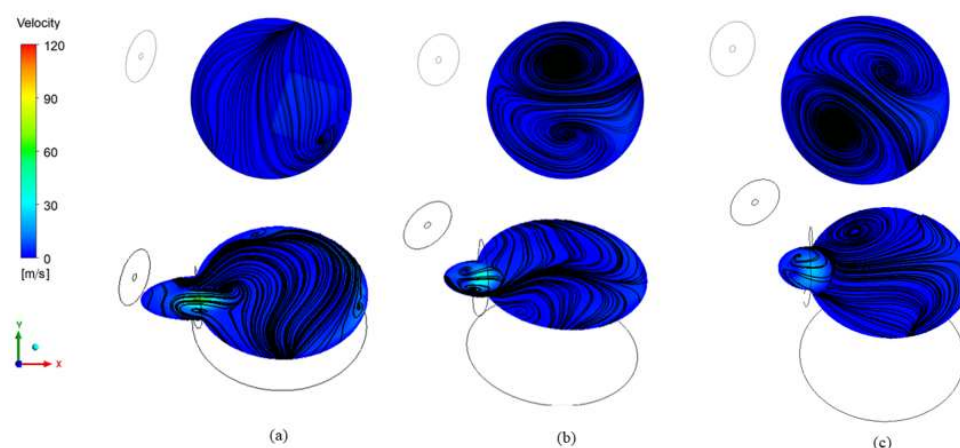


Figure 11. Streamlines inside the reactor chamber, according to the xz plane at the top of the reactor ((**top**) figures) and at the midplane of the jet flow inlet ((**bottom**) figures): (a) 30° ; (b) 50° ; (c) 60° .

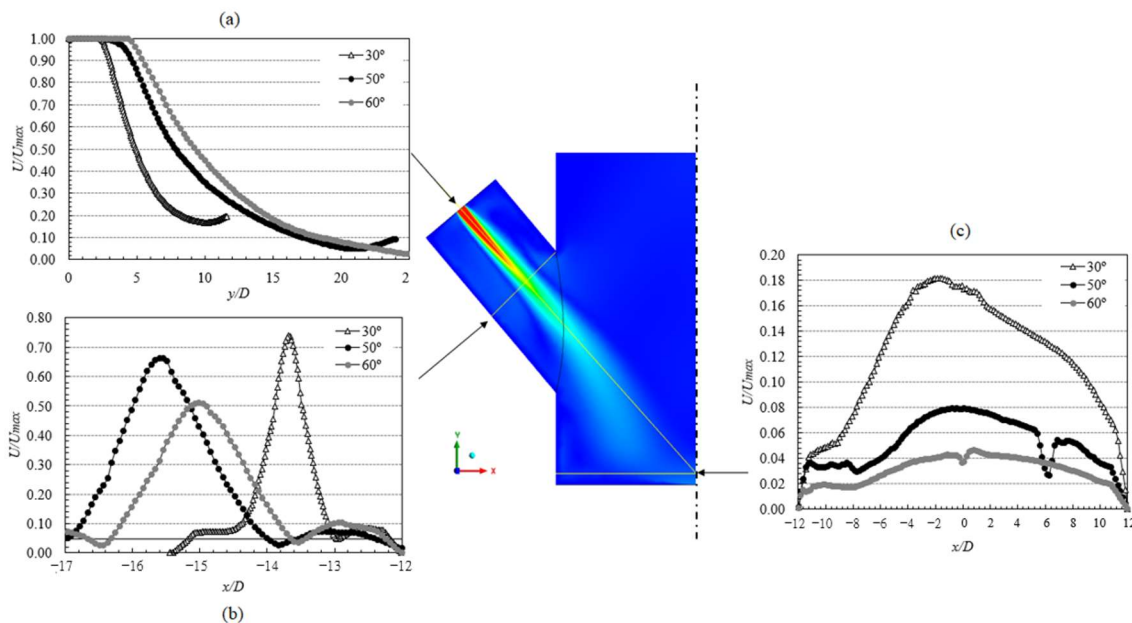


Figure 12. Velocity profiles: (a) at the jet axis; (b) near the intersection between the reactor and the torch exit; (c) near the target surface ($y = 5$ mm).

This velocity profile is directly related to the temperature profiles inside the reactor. The predicted temperature profiles in the previously presented regions are depicted in Figure 13.

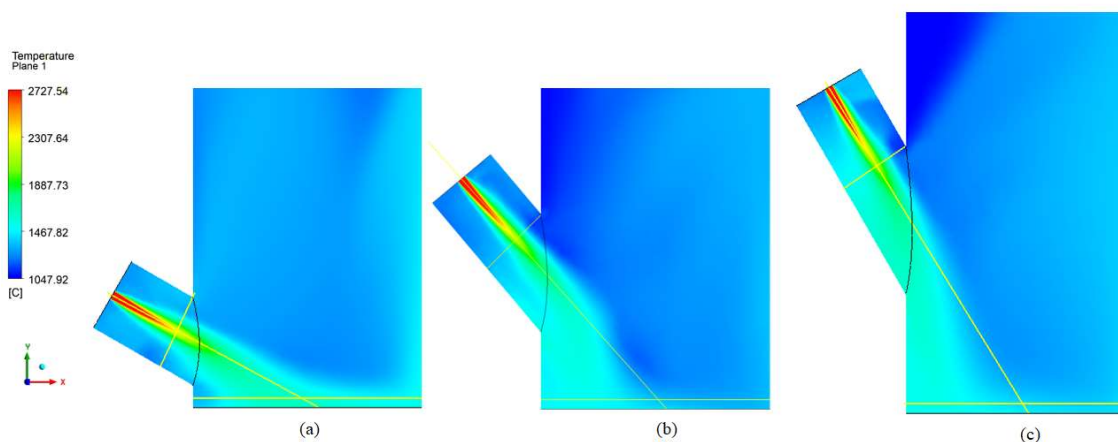


Figure 13. Temperature profile temperatures inside the reactor chamber: (a) 30°; (b) 50°; (c) 60°.

The results expressed in Figure 13 show that the evolution of the velocity profile has a direct influence on the temperature profile, since the temperature profile follows the same trend as the velocity. The results show that higher and uniform temperatures are obtained when the torch is tilted at a 30° angle, and these temperatures decrease as this angle increases.

Looking closely at the velocity profile along the jet axis, as shown in Figure 14a, near to the intersection zone, as shown in Figure 14b, and near the target surface at a distance corresponding to $y = 5$ mm, as shown in Figure 14c, it appears that these results corroborate the previous conclusions. Since the 30° angle allows for greater temperature uniformity in the vicinity of the target surface, reaching values around 10% and 20% higher than the case of 50° and 60°, it is concluded that this angle will ensure greater thermal uniformity and heating temperatures in the sample. Therefore, the angle of 30° is assumed to be the configuration that will optimize the gasification process.

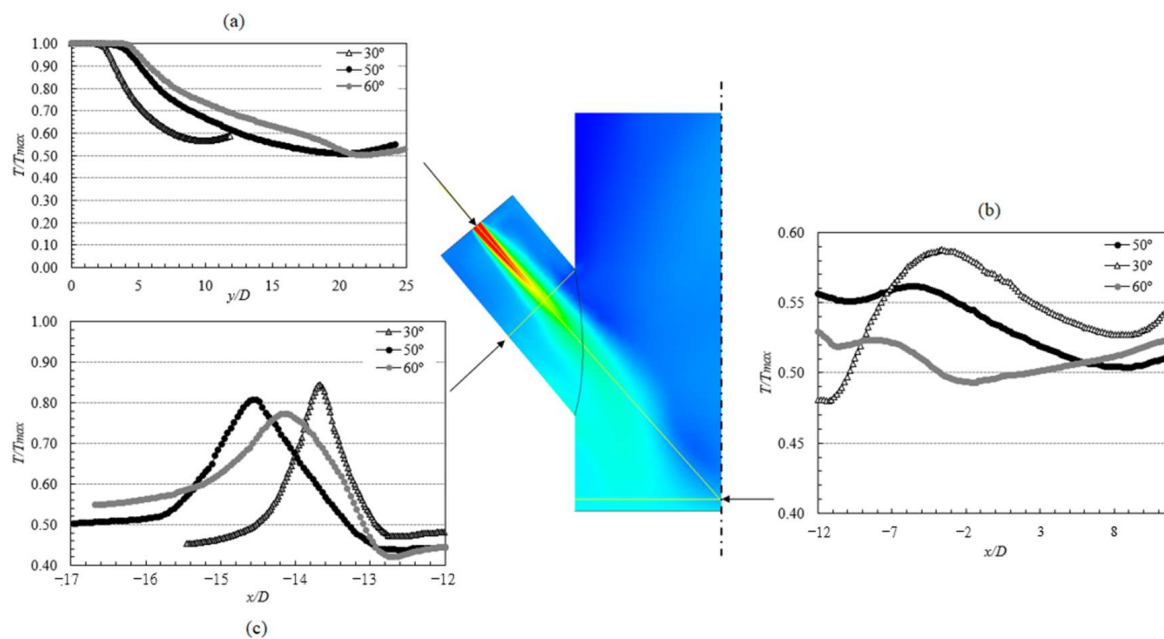


Figure 14. Velocity profiles comparison at various positions: (a) at the jet axis; (b) near the intersection between the reactor and the torch exit; (c) near the target surface ($y = 5$ mm).

3.3.2. Heat Exchanger

As a result of the calculations, a 5.2 kW heat dissipation power was obtained for 19 tubes with a diameter (d) equal to 25 mm (one-tube pass) inside a shell with a 139.7 mm external diameter (D) and 750 mm length (L). Despite the length of the tubes, the gas velocity inside each tube was estimated to be around 2.72 m/s. This means a short residence time of the gas inside HE, at around 0.28 s, ensuring a rapid cooling from 1000 °C to 80 °C. The final design of the HE is presented in Figure 15.

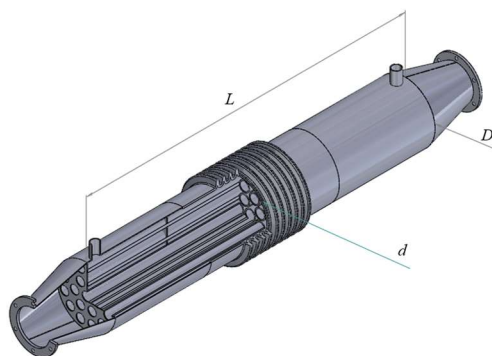


Figure 15. Heat exchanger design.

3.3.3. Scrubber

Based on the calculations conducted for the scrubber, a collection efficiency of 88.5% was obtained, and the application of the Azzopardi and Govan [37] 1D model shows that, to remove all the particles using the presented parameters, a throat length of 120 mm must be ensured. The final validation of the scrubber design consisted of the calculation of the pressure losses based on Leith et al. [39]. The obtained value was about 500 Pa, which is considered acceptable for this type of application. The design of the Venturi scrubber based on this study is depicted in Figure 16.

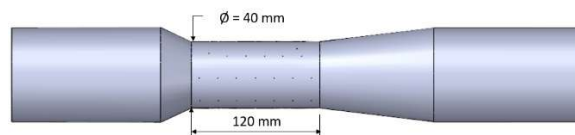


Figure 16. Venturi scrubber configuration.

3.3.4. Particle Separator

The calculations yielded significant results for the cyclonic separator. The capture efficiency was determined to be 0.96, indicating a high effectiveness in capturing particles and droplets from the gas stream. In terms of pressure drop, a value of 0.37 kPa was estimated for the cyclonic separator. This indicates a relatively low pressure drop, which is desirable to ensure efficient operation and minimal energy consumption within the system. The dimensions of the cyclonic separator can be observed in Figure 17, providing a visual representation of its structure and size.

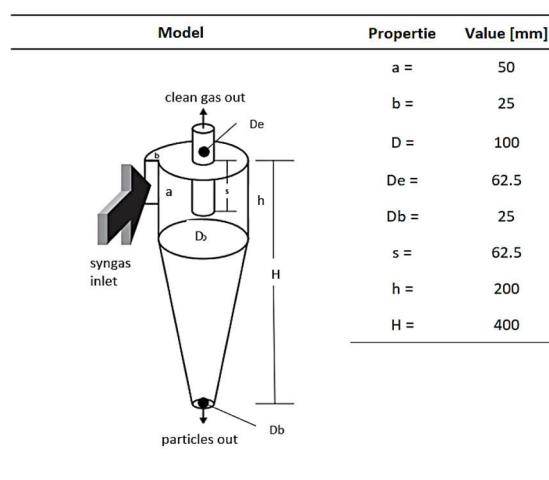


Figure 17. Cyclone configuration.

4. Conclusions

In this work, a comprehensive and detailed study was carried out, focusing on the plasma gasification of sewage sludge, an emerging technology that allows for the conversion of organic waste into syngas in a clean and efficient way. For this, the sewage sludge and its ashes were characterized in terms of their thermogravimetric, physicochemical, and thermal properties. The results showed that the sewage sludge has a high calorific value (LHV = 20.78 MJ/kg), a high carbon and hydrogen content (C = 57.2%, H = 8.42%), a low sulfur content (S = 0.46%), and an ash content of 18%. These properties indicate that sewage sludge is a suitable raw material for use in the gasification process. Additionally, the resulting ashes have a low melting temperature (1350 °C), which determines their ability to melt and flow out of the gasification reactor.

Knowledge of the behavior of the raw material is crucial for the design of an experimental plasma gasification system and the different modules that constitute it, such as the reactor, heat exchanger, scrubber, and cyclone. The system was designed and optimized considering the impacts and properties of sewage sludge, as well as the numerical simulations that were carried out to investigate the influence of the plasma torch angle on the temperature and speed profile within the reactor. It was discovered that the optimal angle of the plasma torch is 30°, as this allows for higher and more uniform heating over the bottom surface where the sample will be placed, optimizing the gasification process. According to the simulations, the maximum temperature reached in the reactor was 1467 °C. For the heat exchanger, a heat dissipation of 5.2 kW was determined, with a total of 19 tubes of 25 mm diameter inside a shell with an external diameter of 139.7 mm and a length of

750 mm. The collection efficiency of the scrubber was estimated to be 88.5%, with a pressure of approximately 500 Pa. For the particle separator, we achieved a capture efficiency of 96%, with a pressure drop of 0.37 kPa. This study significantly contributes to the advancement of knowledge and the technology of plasma gasification, providing valuable information for the design and operation of the gasification system. This work is an important step for the application of plasma gasification in the management of sewage sludge waste and in the production of sustainable energy.

Author Contributions: Conceptualization, F.O., L.M., J.C.T. and C.V.; formal analysis, N.P. and F.V.B.; investigation, N.P., A.R., F.P. and F.V.B.; methodology, N.P., A.R., F.P. and F.V.B.; project administration, F.O. and C.V.; resources, F.O., J.C.T. and C.V.; software, N.P. and F.V.B.; supervision, L.M., J.C.T. and C.V.; validation, N.P., A.R., F.P. and F.V.B.; writing—original draft, N.P. and F.V.B.; writing—review and editing, L.M., J.C.T. and C.V. All authors have read and agreed to the published version of the manuscript.

Funding: This work has been co-financed by the European Union through the European Regional Development Fund (ERDF), under the COMPETE 2020—Operational Program for Competitiveness and Internationalization, Portugal 2020, within the scope of the project Plasma2Gas: New Energy Level—Gasification System (POCI-01-0247-FEDER-070233).

Data Availability Statement: The data presented in this study are available on request from the corresponding author due to confidentiality reasons.

Conflicts of Interest: The authors declare no conflicts of interest. The funders had no role in the design of the study; in the collection, analyses, or interpretation of data; in the writing of the manuscript, or in the decision to publish the results.

Nomenclature

Acronyms		SI Unit
WWT	Wastewater treatment	
SS	Sewage sludge	
WWTPs	Wastewater treatment plants	
db	Dry basis	
CGE	Cold gas efficiency	(%)
CCE	Carbon conversion efficiency	(%)
HE	Heat exchanger	
LHV	Low heating value	(MJ/kg)
HHV	High heating value	(MJ/kg)
TGA	Thermogravimetric analysis	
DSC	Differential Scanning Calorimetry	
XRF	X-ray fluorescence spectroscopy	
LDT	Laser Diffraction Technique	
SMD	Sauter Mean Diameter	
Symbol	Quantity	SI Unit
C_p	Specific heat capacity	(J/kgK)
P	Power	(kW)
D, d	Diameter	(m)
G_k	Generation of k	(kg/m ³ ·s ³)
G_ω	Generation of ω	(kg/m ³ ·s ²)
H	Nozzle-to-plate distance	(m)
k	Turbulent kinetic energy; thermal conductivity	(m ² /s ²); (W/mK)
p	Pressure	(Pa)
r	Radius	(m)
Re	Reynolds number	-
S_k, S_ω	Source term	(W/m ³)
t	Time	(s)
T	Temperature	(°C)
u, U	Velocity	(m/s)
$x, y,$	Cartesian coordinates	-

Greek Symbol		
Γ_k, Γ_ω	Effective diffusivity of k, ω	(kg/m·s)
α	Thermal diffusivity	(m ² /s)
θ	Characteristic time	-
μ	Dynamic viscosity	(Pa·s)
ρ	Density	(kg/m ³)
τ	Dimensionless time	-
ω	Specific dissipation rate	(1/s)
Subscript		
max	Maximum	
min	Minimum	
w	Wall	

References

- Ronda, A.; Haro, P.; Gómez-Barea, A. Sustainability assessment of alternative waste-to-energy technologies for the management of sewage sludge. *Waste Manag.* **2023**, *159*, 52–62. [CrossRef] [PubMed]
- Database-Eurostat. Available online: https://ec.europa.eu/eurostat/data/database?node_code=env_ww_spd (accessed on 19 May 2023).
- Bagheri, M.; Bauer, T.; Burgman, L.E.; Wetterlund, E. Fifty years of sewage sludge management research: Mapping researchers' motivations and concerns. *J. Environ. Manag.* **2023**, *325*, 116412. [CrossRef] [PubMed]
- Ali, A.M.; Hassan, M.A.A.; Abdulkarim, B.I. Thermal Plasma: A Technology for Efficient Treatment of Industrial and Wastewater Sludge. *IOSR J. Environ. Sci.* **2016**, *10*, 63–75.
- Wnukowski, M.; Kordylewski, W.; Łuszkiewicz, D.; Leśniewicz, A.; Ociepa, M.; Michalski, J. Sewage Sludge-Derived Producer Gas Valorization with the Use of Atmospheric Microwave Plasma. *Waste Biomass-Valorization* **2020**, *11*, 4289–4303. [CrossRef]
- Oliveira, M.; Ramos, A.; Ismail, T.M.; Monteiro, E.; Rouboa, A. A Review on Plasma Gasification of Solid Residues: Recent Advances and Developments. *Energies* **2022**, *15*, 1475. [CrossRef]
- Gomez, E.; Rani, D.A.; Cheeseman, C.; Deegan, D.; Wise, M.; Boccaccini, A. Thermal plasma technology for the treatment of wastes: A critical review. *J. Hazard. Mater.* **2009**, *161*, 614–626. [CrossRef]
- Speight, J.G. *Handbook of Gasification Technology*; Wiley: Hoboken, NJ, USA, 2020; ISBN 9781118773536.
- Zhovtyansky, V.; Valinčius, V. Efficiency of Plasma Gasification Technologies for Hazardous Waste Treatment. In *Gasification Low-Grade Feed*; IntechOpen: London, UK, 2018. [CrossRef]
- Erdogan, A.A.; Yilmazoglu, M.Z. Experimental and numerical investigation of medical waste disposal via plasma gasification. *Appl. Energy* **2024**, *353*, 122014. [CrossRef]
- Gao, N.; Kamran, K.; Quan, C.; Williams, P.T. Thermochemical conversion of sewage sludge: A critical review. *Prog. Energy Combust. Sci.* **2020**, *79*, 100843. [CrossRef]
- Pacheco, N.; Barbosa, F.V.; Ribeiro, A.; Carvalho, J.; Nascimento, L.; Soares, M.; Valerio, N.; Faria, L.; Silva, A.; Araujo, J.; et al. An Experimental Setup for Plasma Gasification of Sewage Sludge. In Proceedings of the 8th Thermal and Fluids Engineering Conference (TFEC), College Park, MD, USA, 26–29 March 2023; pp. 543–557. [CrossRef]
- Zheng, Q.; Kaur, S.; Dames, C.; Prasher, R.S. Analysis and improvement of the hot disk transient plane source method for low thermal conductivity materials. *Int. J. Heat Mass Transf.* **2020**, *151*, 119331. [CrossRef]
- Trofimov, A.A.; Atchley, J.; Shrestha, S.S.; Desjarlais, A.O.; Wang, H. Evaluation of measuring thermal conductivity of isotropic and anisotropic thermally insulating materials by transient plane source (Hot Disk) technique. *J. Porous Mater.* **2020**, *27*, 1791–1800. [CrossRef]
- He, Y. Rapid thermal conductivity measurement with a hot disk sensor: Part 1. Theoretical considerations. *Thermochim. Acta* **2005**, *436*, 122–129. [CrossRef]
- Eshel, G.; Levy, G.J.; Mingelgrin, U.; Singer, M.J. Critical evaluation of the use of laser diffraction for particle-size distribution analysis. *Soil Sci. Soc. Am. J.* **2004**, *68*, 736–743. [CrossRef]
- Kowalczyk, P.B.; Drzymala, J. Physical meaning of the Sauter mean diameter of spherical particulate matter. *Part. Sci. Technol.* **2016**, *34*, 645–647. [CrossRef]
- Wang, P.; Massoudi, M. Slag behavior in gasifiers. Part I: Influence of coal properties and gasification conditions. *Energies* **2013**, *6*, 784–806. [CrossRef]
- Deutsches Institut für Normung e.V. (DIN). *DIN 51730:2022-02. Testing of Solid Fuels-Determination of Ash Fusibility*; Deutsche Institut für Normung e.V. (DIN): Berlin, Germany, 2022.
- Basu, P. *Biomass Gasification, Pyrolysis and Torrefaction: Practical Design and Theory*; Academic Press: Cambridge, MA, USA, 2018.
- Menter, F.R. Two-equation eddy-viscosity turbulence models for engineering applications. *AIAA J.* **1994**, *32*, 1598–1605. [CrossRef]
- Brakmann, R.; Chen, L.; Weigand, B.; Crawford, M. Experimental and Numerical Heat Transfer Investigation of an Impinging Jet Array on a Target Plate Roughened by Cubic Micro Pin Fins. *J. Turbomach.* **2016**, *138*, 111010. [CrossRef]
- Guo, Q.; Wen, Z.; Dou, R. Experimental and numerical study on the transient heat-transfer characteristics of circular air-jet impingement on a flat plate. *Int. J. Heat Mass Transf.* **2017**, *104*, 1177–1188. [CrossRef]

24. Issac, J.; Singh, D.; Kango, S. Experimental and numerical investigation of heat transfer characteristics of jet impingement on a flat plate. *Heat Mass Transf.* **2020**, *56*, 531–546. [CrossRef]
25. Singh, A.; Chakravarthy, B.; Prasad, B. Numerical simulations and optimization of impinging jet configuration. *Int. J. Numer. Methods Heat Fluid Flow* **2021**, *31*, 1–25. [CrossRef]
26. Lu, S.; Deng, Q.; Ligrani, P.M.; Jiang, H.; Zhang, Q. Effects of coolant and wall temperature variations on impingement jet array thermal performance. *Numer. Heat Transfer, Part A Appl.* **2021**, *79*, 68–82. [CrossRef]
27. Barbosa, F.V.; Teixeira, S.F.C.F.; Teixeira, J.C.F. Numerical analysis of the influence of the jet-to-jet spacing between two adjacent air jets impinging a flat plate. In Proceedings of the 4th Thermal and Fluids Engineering Conference, Las Vegas, NV, USA, 14–17 April 2019.
28. ANSYS. *Ansys Fluent Theory Guide*; ANSYS, Inc.: Canonsburg, PA, USA, 2013; pp. 1–759. [CrossRef]
29. Cengel, Y.A.; Ghajar, A.J. *Heat and Mass Transfer: Fundamentals and Applications*, 5th ed.; McGraw-Hill Education: New York, NY, USA, 2011.
30. Rhie, C.M.; Chow, W.L. Numerical Study of the Turbulent Flow Past an Airfoil with Trailing Edge Separation. *AIAA J.* **1983**, *21*, 1525–1532. [CrossRef]
31. Ferziger, J.H.; Peric, M. *Computational Methods for Fluid Dynamics. Computational Methods for Fluid Dynamics*, 3rd ed.; Springer: New York, NY, USA, 1996.
32. de Alencar Júnior, N.R.; Gabaí, I. Incineração e dioxinas: Análise do aporte teórico disponível. Ano de Publicação Desconhecido. Autores Nehemias Rodrigues de Alencar Júnior e Isaac Gabaí. no. Mvc, 2011. Available online: https://www.abepro.org.br/biblioteca/ENEGEP2001_TR104_0410.pdf (accessed on 9 April 2024).
33. Araújo, S.; Silva, R. Estudo da Formação de Dioxinas e Furanos em Sistemas Auxiliares de Plantas de Cimento que Usam o Co-Processamento de Resíduos Combustíveis. *Ii Congr. Nac. Eng. Mecânica* **2002**, *10*. Available online: <http://www.abcm.org.br/app/webroot/anais/conem/2002/trabalhos/tema03/CPB0181.pdf> (accessed on 21 March 2023).
34. Cengel, Y.; Turner, R.; Cimbala, J. *Fundamental of Thermal Fluid Sciences*, 5th ed.; McGraw-Hill Education: New York, NY, USA, 2008.
35. Menzel, D.B. *EPA Air Pollution Standard*, 6th ed.; United States Environmental Protection Agency: Washington, DC, USA, 2002.
36. Bretschneider, B.; Kurfurst, J. *Air Pollution Control Technology*; Elsevier Science: Amsterdam, The Netherlands, 1987.
37. Azzopardi, B.J.; Govan, A.H. The Modeling of Venturi Scrubbers. *Filtr. Sep.* **1984**, *21*, 1984.
38. Hesketh, H.E.; Mohan, K. Specifying venturi scrubber throat length for effective particle capture at minimum pressure loss penalty. *J. Air Pollut. Control. Assoc.* **1983**, *33*, 854–857. [CrossRef]
39. Miller, P.C.H.; Tuck, C.R.; Murphy, S.; Ferreira, M.C. Measurements of the droplet velocities in sprays produced by different designs of agricultural spray nozzle. In Proceedings of the 22nd European Conference on Liquid Atomization and Spray Systems, Como Lake, Italy, 8–10 September 2008.
40. Maurício, P.; Silva, P.; Fonseca, A.; Duarte, P. Um Algoritmo para Dimensionamento de Ciclones. *Rev. Fac. Ciência Tecnol.* **2006**. Available online: <https://bdigital.ufp.pt/handle/10284/539> (accessed on 9 April 2024).
41. Wang, L.K.; Pereira, N.C.; Hung, Y.-T. *Handbook of Environmental Engineering-Air Pollution Engineering*; Humana Press, Inc: Totowa, NJ, USA, 2004.
42. EPA Technology Assessment Report Aqueous Sludge Gasification Technologies. Epa/600/R-12/540, no. June. 2012; pp. 1–58. Available online: <https://nepis.epa.gov/Exe/ZyPDF.cgi/P100EM1Q.PDF?Dockey=P100EM1Q.PDF> (accessed on 9 April 2024).
43. Chun, Y.N.; Song, H.G. Microwave-enhanced gasification of sewage sludge waste. *Environ. Eng. Res.* **2018**, *24*, 591–599. [CrossRef]
44. Werle, S.; Dudziak, M. 25-Gasification of sewage sludge. *Ind. Munic. Sludge Emerg. Concerns Scope Resour. Recover.* **2019**, 575–593. [CrossRef]
45. Bora, R.R.; Richardson, R.E.; You, F. Resource recovery and waste-to-energy from wastewater sludge via thermochemical conversion technologies in support of circular economy: A comprehensive review. *BMC Chem. Eng.* **2020**, *2*, 8. [CrossRef]
46. Fedelich, N. *Thermal Analysis in Practice-Tips and Hints*. Mattler Toledo: Schwerzenbach, Switzerland, 2016.
47. Wang, K.-S.; Tseng, C.-J.; Chiou, I.-J.; Shih, M.-H. The thermal conductivity mechanism of sewage sludge ash lightweight materials. *Cem. Concr. Res.* **2005**, *35*, 803–809. [CrossRef]
48. Song, H.W.; Park, K.J.; Han, S.K.; Jung, H.S. Thermal conductivity characteristics of dewatered sewage sludge by thermal hydrolysis reaction. *J. Air Waste Manag. Assoc.* **2014**, *64*, 1384–1389. [CrossRef]
49. Rawle, A.F. Basic of principles of particle-size analysis. *Surf. Coat. Int. Part A Coat. J.* **2003**, *86*, 58–65.
50. Barbosa, F.V.; Teixeira, S.F.; Teixeira, J.C. Convection from multiple air jet impingement-A review. *Appl. Therm. Eng.* **2023**, *218*, 119307. [CrossRef]
51. Hrycak, P.; Lee, D.T.; Gauntner, J.W.; Livingood, J.N.B. Experimental Flow Characteristics of a Single Turbulent Jet Impinging on a Flat Plate. Available online: <https://ntrs.nasa.gov/citations/19700011262> (accessed on 2 September 2013).

Disclaimer/Publisher’s Note: The statements, opinions and data contained in all publications are solely those of the individual author(s) and contributor(s) and not of MDPI and/or the editor(s). MDPI and/or the editor(s) disclaim responsibility for any injury to people or property resulting from any ideas, methods, instructions or products referred to in the content.